Rashba spin-orbit coupling effects in $Cd_{1-x}Mn_xTe$ quantum dots

F. M. Hashimzade, A. M. Babayev, and B. H. Mehdiyev*
Institute of Physics, National Academy of Sciences of Azerbaijan, AZ 1143, Baku, Azerbaijan
(Received 21 December 2005; revised manuscript received 6 March 2006; published 16 June 2006)

We present a theoretical study of the electronic structure of a $Cd_{1-y}Mn_yTe$ quantum dot with Rashba spin-orbit coupling in the presence of a magnetic field. The multiband $\mathbf{k}\cdot\mathbf{p}$ theory is used to describe electrons in Rashba spin-orbit coupling regimes and an external magnetic field, taking into account the $sp-d$ exchange interaction between the carriers and the magnetic ions. We calculated the radius, the thickness, and the magnetic field dependence of Rashba splitting for electrons. We find that the energy levels of electrons for different Mn concentrations exhibit quite different behavior as a function of magnetic field.

DOI: 10.1103/PhysRevB.73.245321 PACS number(s): 71.70.Ej, 71.70.Di, 71.70.Gm, 71.20.Nr

I. INTRODUCTION

Spin-dependent phenomena have recently attracted considerable and continuous attention as they are the key concept in modern spintronics. A spin field-effect transistor proposed by Datta and Das[1] is based on the fact that spin precession can be controlled by an external field due to the spin-orbit interaction. In a crystal with bulk inversion asymmetry (BIA) the energy bands are spin split for a given direction of the wave vector $\mathbf{k}$. In semiconductor heterostructures the spin splitting may also occur[2] as a result of the structural inversion asymmetry (SIA), as was discussed in an early paper by Rashba.[3] Novel spin properties arise from the interplay between Rashba spin splitting and further confinement of two-dimensional electrons in quantum wires[4–7] or dots.[8–11] In Refs. 12–14 a solution was found to the problem of the Rashba spin-orbit coupling in semiconductor quantum dots, and the energy spectrum, wave functions, and spin-flip relaxation times were calculated using perturbation theory. Additionally, the spin splitting of the subbands can be enhanced by introducing magnetic ions (Mn) in the quantum well, quantum wire, and quantum dot structures, e.g., $Cd_{1-y}Mn_yTe$ diluted magnetic semiconductor (DMS) structures.

DMS provides us with an interesting possibility for tailoring the spin splitting and the spin polarization due to the strong $sp-d$ exchange interaction between the carriers and the local magnetic ions.[15,16] The spin splitting in the DMS system can be tuned by changing the external magnetic field. DMSs are among the best candidates to combine semiconductor electronics with magnetism. In DMS the Lande g factor is a function of the applied magnetic field, the temperature, and the molar fraction y.[17] For instance, for low field values $g(H\to 0)=-0.5$ in CdTe and $g(H\to 0)=+100$ in $Cd_{0.98}Mn_{0.02}Te$ at helium temperatures. Recently, the incorporation of Mn ions into the crystal matrix of different II-VI semiconductors lead to the successful fabrication of DMS quantum dots and magnetic DMS hybrid structures.[18–23] Low-dimensional DMS structures have been the subject of a few studies.[24–27] The electron and hole states in DMS quantum dots have been investigated in Ref. 25. The optical properties of DMS quantum dots were studied within the framework of the effective-mass theory.[26] The band structure of the semimagnetic $Hg_{1-y}Mn_yTe$ quantum well has been calculated in Ref. 28.

In this paper we present a theoretical study of the electronic structure of a DMS cylindrical quantum dot with Rashba spin-orbit coupling in weak and quantizing magnetic fields. The calculation is done using the multiband $\mathbf{k}\cdot\mathbf{p}$ theory and taking into account the $sp-d$ interaction between the carriers and the magnetic ions. Numerical results are presented for $Cd_{1-y}Mn_yTe$ quantum dots. The results were compared with a nonmagnetic semiconductor (NMR) CdTe (Mn free case $y=0$) quantum dot. The paper is organized as follows. In Sec. II the theoretical model and formalism are presented. In Sec. II A we consider the model for nonquantizing as well as for zero external magnetic fields. In Sec. II B the electron levels in the quantizing magnetic field are considered. In Sec. III we present the numerical results along with the discussion. A brief conclusion is given in Sec. IV.

II. MODEL AND FORMALISM

We consider the Kane type DMS $Cd_{1-y}Mn_yTe$ quantum dot with the z axis along the growth direction. We describe the confinement of electrons in quantum dots by a separable potential $V(\vec{r})=V(z)+V(x,y)$, where $V(x,y)$ is the confinement potential in the xy plane and $V(z)$ is the potential in the z direction. The confining potential in the xy plane is assumed to be symmetric, $V(x,y)=V(\rho)$. Here we will mainly consider a hard-wall confining potential in the xy plane, $V(\rho)=\infty$ for $\rho>r_0$ and $V(\rho)=0$ for $\rho<r_0$, r_0 being the radius of the quantum dot. The perpendicular confinement $V(z)$ is assumed strong enough that only the lowest z-subband is occupied. Here $V(z)$ is assumed to be asymmetric. We consider an eight-band $\mathbf{k}\cdot\mathbf{p}$ model of the band structure at $k=0$ (Γ *point*). The Γ_6 subband is separated by the energy gap ε_g from the fourfold degenerate Γ_8 subband $[\varepsilon_g=\varepsilon(\Gamma_6)-\varepsilon(\Gamma_8)]$, which is, in turn, split off by the spin-orbit interaction Δ from the Γ_7 subband $[\Delta=\varepsilon(\Gamma_8)-\varepsilon(\Gamma_7)]$. The spin-orbit interaction for the Γ_6 conduction band is given by Rashba term[29,30]

$$H_{6c}^{SO}=\frac{1}{2}R_c([\mathbf{n}\times\mathbf{k}]\cdot\sigma), \tag{1}$$

where k is the momentum operator, R_c is the coupling strength for conduction band, $\mathbf{n}$ is the unit vector in the growth direction, and $\sigma=(\sigma_x,\sigma_y,\sigma_z)$ denotes the Pauli spin matrices.

The Rashba model (1) can be derived by purely group-theoretical means. The electron states in the lowest conduction band are S like (orbital angular momentum $l=0$). With spin-orbit (SO) interaction the total angular momentum is $j=1/2$. Both $\mathbf{k}$ and $\mathbf{n}$ are polar vectors and $[\mathbf{n}\times\mathbf{k}]$ is an axial vector. Likewise, the spin matrices $\sigma_x,\sigma_y,\sigma_z$ form an axial vector σ. The dot product (1) of $[\mathbf{n}\times\mathbf{k}]$ and σ therefore transforms according to the identity representation Γ_1, in accordance with the theory of invariants of Bir and Pikus.[31] In the Γ_6 conduction band the scalar triple product (1) is the only term that is compatible with the symmetry of the band.

Here, we will neglect the bulk inversion asymmetry (Dresselhaus effect) and consider only the structure inversion asymmetry, as the latter can dominate in quantum dots obtained in a heterostructure[8,9] of interest in this paper.

In CdTe-based structures, the strong coupling between the s-like conduction and p-like valence band causes mixing of the electronic states and induces nonparabolicity in the conduction bands. These effects were taken into account by Kane in the framework of the $\mathbf{k}\cdot\mathbf{p}$ theory.[32] In order to consider the coupling between the Γ_7, Γ_8, and Γ_6 subbands we choose usual eight-band Bloch basis set[33]

$$U_1(\mathbf{r})=iS\nu_1,\quad U_2(\mathbf{r})=iS\nu_2,$$

$$U_3(\mathbf{r})=-\frac{1}{\sqrt{2}}(X+iY)\nu_1,$$

$$U_4(\mathbf{r})=-\frac{1}{\sqrt{6}}[(X+iY)\nu_2-2Z\nu_1],$$

$$U_5(\mathbf{r})=\frac{1}{\sqrt{6}}[(X-iY)\nu_1+2Z\nu_2],$$

$$U_6(\mathbf{r})=\frac{1}{\sqrt{2}}(X-iY)\nu_2,$$

$$U_7(\mathbf{r})=-\frac{1}{\sqrt{3}}[(X+iY)\nu_2+Z\nu_1],$$

$$U_8(\mathbf{r})=\frac{1}{\sqrt{3}}[(X-iY)\nu_1-Z\nu_2], \tag{2}$$

where

$$\nu_1=\begin{pmatrix}1\\0\end{pmatrix}\ \text{and}\ \nu_2=\begin{pmatrix}0\\1\end{pmatrix}$$

are spin functions corresponding, respectively, to up and down. For the chosen basis set, the Kane Hamiltonian neglecting quadratic terms takes the following form:

$$H_{kp}=\begin{pmatrix}
-\varepsilon & 0 & -\frac{Pk_+}{\sqrt{2}} & \sqrt{\frac{2}{3}}Pk_z & \frac{Pk_-}{\sqrt{6}} & 0 & -\frac{Pk_z}{\sqrt{3}} & \frac{Pk_-}{\sqrt{3}}\\
0 & -\varepsilon & 0 & -\frac{Pk_+}{\sqrt{6}} & \sqrt{\frac{2}{3}}Pk_z & \frac{Pk_-}{\sqrt{2}} & -\frac{Pk_+}{\sqrt{3}} & -\frac{Pk_z}{\sqrt{3}}\\
-\frac{Pk_-}{\sqrt{2}} & 0 & -\varepsilon-\varepsilon_g & 0 & 0 & 0 & 0 & 0\\
\sqrt{\frac{2}{3}}Pk_z & -\frac{Pk_-}{\sqrt{6}} & 0 & -\varepsilon-\varepsilon_g & 0 & 0 & 0 & 0\\
\frac{Pk_+}{\sqrt{6}} & \sqrt{\frac{2}{3}}Pk_z & 0 & 0 & -\varepsilon-\varepsilon_g & 0 & 0 & 0\\
0 & \frac{Pk_+}{\sqrt{2}} & 0 & 0 & 0 & -\varepsilon-\varepsilon_g & 0 & 0\\
-\frac{Pk_z}{\sqrt{3}} & -\frac{Pk_-}{\sqrt{3}} & 0 & 0 & 0 & 0 & -\Delta-\varepsilon-\varepsilon_g & 0\\
\frac{Pk_+}{\sqrt{3}} & -\frac{Pk_z}{\sqrt{3}} & 0 & 0 & 0 & 0 & 0 & -\Delta-\varepsilon-\varepsilon_g
\end{pmatrix}, \tag{3}$$

where $P=-i\frac{\hbar}{m_0}\langle S|p_z|Z\rangle$ is the Kane momentum matrix element and $k_\pm=k_x\pm ik_y$, $\mathbf{k}=-i\nabla$. The energy origin has been chosen at the conduction-band minima.

In the presence of a magnetic field, the $sp-d$ exchange interaction of the S and p band electrons with the $3d^5$ electrons of Mn^{2+} in the $Cd_{1-y}Mn_yTe$ layer influences the band structure of the quantum dot. Such an interaction can be taken into account by adding an appropriate exchange term H_{ex} to the Hamiltonian in accordance with Refs. 16 and 17,

$$H_{ex}=\sum_{\mathbf{R}_i} J(\mathbf{r}-\mathbf{R}_i)\mathbf{S}_i\sigma, \tag{4}$$

where $\hat{\mathbf{S}}_i$ and σ are spin operators of the ith magnetic ion (say, Mn^{2+} in $Cd_{1-y}Mn_yTe$) and band electrons, $J(\mathbf{r}-\mathbf{R}_i)$ is the electron-ion exchange integral, and vectors $\mathbf{r}$ and $\mathbf{R}_i$ define the coordinates of the band electron and of the Mn^{2+} ions. In Eq. (4) the sum is taken over all Mn^{2+} ions. Since the electron wave function is extended, the spin operator $\hat{\mathbf{S}}_i$ can be replaced by the thermal average over all states of Mn moments $\langle S_z\rangle$ for a magnetic field in z direction (mean field approximation). Furthermore, within the virtual crystal approximation, $J(\mathbf{r}-\mathbf{R}_i)$ can be replaced by $yJ(\mathbf{r}-\mathbf{R})$, where y is the mole fraction of Mn, and the sum is now taken over all cation sites.[16] The exchange term (4) then becomes

$$H_{ex}=y\sigma_z\langle S_z\rangle\sum_{\mathbf{R}} J(\mathbf{r}-\mathbf{R}). \tag{5}$$

The thermodynamic average $\langle S_z\rangle$ of the z-component of a localized Mn spin in the approximation of noninteracting magnetic moments is determined by the empirical expression[16,17]

$$\langle S_z\rangle=-S_0B_{5/2}\left(\frac{Sg_{\mathrm{Mn}}\mu_BH}{k_B(T+T_0)}\right), \tag{6}$$

where $B_{5/2}(\xi)$ is the Brillouin function, $S=5/2$ corresponds to the spins of the localized $3d^5$ electrons of the Mn^{2+} ions, g_{Mn} is the g-factor of Mn, and k_B is the Boltzmann constant. The effective spin S_0 and the effective temperature $T+T_0$ account for the existence of clusters and antiferromagnetic interaction between Mn ions. The H_{ex} matrix in terms of the above Bloch functions has the form

$$H_{ex}=\begin{pmatrix}
3Ar & 0 & 0 & 0 & 0 & 0 & 0 & 0\\
0 & -3Ar & 0 & 0 & 0 & 0 & 0 & 0\\
0 & 0 & 3A & 0 & 0 & 0 & 0 & 0\\
0 & 0 & 0 & A & 0 & 0 & -2\sqrt{2}A & 0\\
0 & 0 & 0 & 0 & -A & 0 & 0 & 2\sqrt{2}A\\
0 & 0 & 0 & 0 & 0 & -3A & 0 & 0\\
0 & 0 & 0 & -2\sqrt{2}A & 0 & 0 & -A & 0\\
0 & 0 & 0 & 0 & 2\sqrt{2}A & 0 & 0 & A
\end{pmatrix}, \tag{7}$$

where

$$A=\frac{1}{6}N_0\beta y\langle S_z\rangle, \tag{8}$$

$$\beta=\langle X|J|X\rangle=\langle Y|J|Y\rangle=\langle Z|J|Z\rangle, \tag{9}$$

$$\alpha=\langle S|J|S\rangle, \tag{10}$$

and

$$r=\frac{\alpha}{\beta}. \tag{11}$$

Here, N_0 is the number of the unit cells per unit volume; and α and β are constants which describe the exchange interaction according to the $s-d$ and $p-d$ exchange integrals, respectively. Usually, the absolute value of $N_0\beta$ is considerably greater than $N_0\alpha$.

A. Electron energy levels in nonquantizing magnetic field

In this section we consider energy levels of DMS QD in nonquantizing magnetic field, where the influence of a magnetic field on electron levels is taken into account only through the contribution of the exchange interaction and Zeeman term. We present the total Hamiltonian as

$$H=H_{kp}+H_{ex}+H_R+H_z^*+V(\vec{r})I, \tag{12}$$

where I is an 8×8 unit matrix. H_z^* and H_R are the Zeeman and Rashba terms, respectively. These terms are 8×8 matrices and have the following nonzero elements

$$(H_z^*)_{11}=s_H^*/2,\quad (H_z^*)_{22}=-s_H^*/2, \tag{13}$$

$$(H_R)_{12}=-\frac{iR_ck_-}{2},\quad (H_R)_{21}=\frac{iR_ck_+}{2}, \tag{14}$$

where

$$s_H^* = g^* \mu_B H, \tag{15}$$

g^* is the electron effective g-factor in CdTe, and μ_B is the Bohr magneton.

We want to apply the Hamiltonian H to the two equations for the Γ_6 conduction band. The wave function Ψ, which is a vector of eight envelope functions $\Psi_1(\mathbf{r}), \ldots, \Psi_8(\mathbf{r})$ is an eigenfunction of Eq. (12). Therefore we should exclude all valence band envelopes, i.e., $\Psi_3(\mathbf{r}), \ldots, \Psi_8(\mathbf{r})$ from Eq. (12). After averaging in the z direction, for the lowest subband we obtain the following set of two equations for the envelopes $\Psi_1(\mathbf{r})$ and $\Psi_2(\mathbf{r})$:

$$\begin{pmatrix} H_{11} + s_H^*/2 - \varepsilon & -iRk_- \\ iRk_+ & H_{22} - s_H^*/2 - \varepsilon \end{pmatrix} \begin{pmatrix} \Psi_1(\mathbf{r}) \\ \Psi_2(\mathbf{r}) \end{pmatrix} = 0, \tag{16}$$

where $R = 2R_c$ and

$$H_{11} = 3Ar + \frac{P^2}{2L^-} k_+ k_- + \frac{(F^+ + 2L^+)P^2}{6(D^- M^+ - 2T^2)} k_- k_+ + \frac{(2F^+ + L^+)P^2 \langle k_z^2 \rangle}{3(D^+ M^- - 2T^2)}, \tag{17}$$

$$H_{22} = -3Ar + \frac{P^2}{2L^+} k_- k_+ + \frac{(F^- + 2L^-)P^2}{6(D^+ M^- - 2T^2)} k_+ k_- + \frac{(2F^- + L^-)P^2 \langle k_z^2 \rangle}{3(D^- M^+ - 2T^2)}. \tag{18}$$

In Eq. (16) some terms are proportional to the operator k_z, and after averaging in the z direction these terms are zero because $\langle k_z \rangle = 0$ for a single subband; also, $\langle k_z^2 \rangle \simeq \left(\frac{\pi}{d}\right)^2$, where d is the confinement length in the z direction.[11,42]

Here, the following notations are used:

$$D^{\pm} = \varepsilon + \varepsilon_g + \Delta \pm A, \tag{19}$$

$$F^{\pm} = \varepsilon + \varepsilon_g + \Delta \pm 3A, \tag{20}$$

$$L^{\pm} = \varepsilon + \varepsilon_g \pm 3A, \tag{21}$$

$$M^{\pm} = \varepsilon + \varepsilon_g \pm A, \tag{22}$$

$$T = 2A. \tag{23}$$

We consider a DMS quantum dot modeled as a quantum cylinder with the radius r_0 and the thickness d. Because of the symmetry of the problem it is convenient to use cylindrical coordinates, (ρ, φ).

As the Hamiltonian of Eq. (16) commutes with the z projection of the total momentum operator $\hat{J}_z = L_z + \frac{1}{2}\sigma_z$ and the system is cylindrically symmetric the wave functions can be represented as

$$\begin{pmatrix} \Psi_1(\rho, \varphi) \\ \Psi_2(\rho, \varphi) \end{pmatrix} = \begin{pmatrix} e^{im\varphi} f(\rho) \\ e^{i(m+1)\varphi} g(\rho) \end{pmatrix}, \tag{24}$$

where $m = 0; \pm 1, \pm 2, \ldots$ is the quantum number related to the projection of the angular momentum on the z direction. Substitution of Eqs. (24) into Eqs. (16) yields the following system of second-order ordinary differential equations:

$$\left[\rho^2 \frac{d^2}{d\rho^2} + \rho \frac{d}{d\rho} - \rho^2 r_1^0 + \rho^2 \varepsilon_1^0 - m^2\right] f(\rho) + R_1^0 \rho^2 \left(\frac{d}{d\rho} + \frac{m+1}{\rho}\right) g(\rho) = 0,$$

$$\left[\rho^2 \frac{d^2}{d\rho^2} + \rho \frac{d}{d\rho} + \rho^2 r_2^0 + \rho^2 \varepsilon_2^0 - (m+1)^2\right] g(\rho) - R_2^0 \rho^2 \left(\frac{d}{d\rho} - \frac{m}{\rho}\right) f(\rho) = 0. \tag{25}$$

In Eqs. (25) we have introduced following parameters:

$$r_1^0 = \frac{(3Ar + s_H^*/2)}{P^2 \left(\frac{1}{2L^-} + \frac{F^+ + 2L^+}{6(D^- M^+ - 2T^2)}\right)}, \tag{26}$$

$$r_2^0 = \frac{(3Ar + s_H^*/2)}{P^2 \left(\frac{1}{2L^+} + \frac{F^- + 2L^-}{6(D^+ M^- - 2T^2)}\right)}, \tag{27}$$

$$\varepsilon_1^0 = \frac{\varepsilon}{P^2 \left(\frac{1}{2L^-} + \frac{F^+ + 2L^+}{6(D^- M^+ - 2T^2)}\right)} - \frac{\frac{(2F^+ + L^+)\langle k_z^2 \rangle}{3(D^+ M^- - 2T^2)}}{\left(\frac{1}{2L^-} + \frac{F^+ + 2L^+}{6(D^- M^+ - 2T^2)}\right)}, \tag{28}$$

$$\varepsilon_2^0 = \frac{\varepsilon}{P^2 \left(\frac{1}{2L^+} + \frac{F^- + 2L^-}{6(D^+ M^- - 2T^2)}\right)} - \frac{\frac{(2F^- + L^-)\langle k_z^2 \rangle}{3(D^- M^+ - 2T^2)}}{\left(\frac{1}{2L^+} + \frac{F^- + 2L^-}{6(D^+ M^- - 2T^2)}\right)}, \tag{29}$$

$$R_1^0 = \frac{\gamma}{P\left(\frac{1}{2L^-} + \frac{F^+ + 2L^+}{6(D^- M^+ - 2T^2)}\right)}, \tag{30}$$

$$R_2^0 = \frac{\gamma}{P\left(\frac{1}{2L^+} + \frac{F^- + 2L^-}{6(D^+ M^- - 2T^2)}\right)}, \tag{31}$$

$$\gamma = \frac{R}{P}. \tag{32}$$

Upon substitution of $x = \nu\rho$, $f(x) = d_1 J_m(x)$ and $g(x) = d_2 J_{m+1}(x)$, where $J_l(\xi)$ is a Bessel function, and using the properties of Bessel functions, we obtain

$$x^2\frac{d^2}{dx^2}J_m(x)+x\frac{d}{dx}J_m(x)+\left(\frac{\varepsilon_1^0-r_1^0}{\nu^2}+\frac{R_1^0}{\nu}\frac{d_2}{d_1}\right)x^2J_m(x)-m^2J_m(x)=0,$$

$$x^2\frac{d^2}{dx^2}J_{m+1}(x)+x\frac{d}{dx}J_{m+1}(x)+\left(\frac{\varepsilon_2^0+r_2^0}{\nu^2}+\frac{R_2^0}{\nu}\frac{d_1}{d_2}\right)x^2J_{m+1}(x)-(m+1)^2J_{m+1}(x)=0. \quad (33)$$

This equation can be satisfied only if

$$\frac{\varepsilon_1^0-r_1^0}{\nu^2}+\frac{R_1^0}{\nu}\frac{d_2}{d_1}=1, \quad (34)$$

$$\frac{\varepsilon_2^0+r_2^0}{\nu^2}+\frac{R_2^0}{\nu}\frac{d_1}{d_2}=1. \quad (35)$$

One can see that for each given value of ε we obtain a biquadratic equation for ν. The solutions of this equation are

$$\nu_\pm=\left[\frac{1}{2}(\varepsilon_2^0+r_2^0+\varepsilon_1^0-r_1^0+R_1^0R_2^0)\pm((\varepsilon_2^0+r_2^0+\varepsilon_1^0-r_1^0+R_1^0R_2^0)^2+4(r_1^0\varepsilon_2^0-r_2^0\varepsilon_1^0+r_2^0r_1^0-\varepsilon_1^0\varepsilon_2^0))^{1/2}\right]^{1/2}. \quad (36)$$

Hence there are two degenerate solutions for ν that are combined in the general solution

$$f(\rho)=\tilde{A}d_1^+J_m(\nu_+\rho)+\tilde{B}d_1^-J_m(\nu_-\rho),$$

$$g(\rho)=\tilde{A}d_2^+J_{m+1}(\nu_+\rho)+\tilde{B}d_2^-J_{m+1}(\nu_-\rho). \quad (37)$$

In a cylindrical quantum dot with infinite potential barrier the radial part of the wave function must vanish at the boundary: $f(\rho=r_0)=g(\rho=r_0)=0$. This condition determines the energy spectrum of electrons in DMS QD in a weak magnetic field.

$$\frac{d_1^+d_2^-}{d_2^+d_1^-}J_m(\nu_+r_0)J_{m+1}(\nu_-r_0)-J_m(\nu_-r_0)J_{m+1}(\nu_+r_0)=0, \quad (38)$$

where

$$\frac{d_1^+d_2^-}{d_2^+d_1^-}=\frac{(\nu_+^2-\varepsilon_2^0-r_2^0)(\nu_-^2-\varepsilon_1^0+r_1^0)}{\nu_+\nu_-R_1^0R_2^0}. \quad (39)$$

The nth solution of this equation defines the energy of the nth electron level with the angular momentum projection m and total angular momentum $j_z=m+1/2$.

In the absence of the Zeeman and exchange interaction term we have $\frac{d_1^+d_2^-}{d_2^+d_1^-}=1$, so that Eq. (38) simplifies to

$$J_m(\nu_+r_0)J_{m+1}(\nu_-r_0)-J_m(\nu_-r_0)J_{m+1}(\nu_+r_0)=0. \quad (40)$$

Because for Bessel functions $J_n(z)=(-1)^nJ_{-n}(z)$, Eq. (40) is invariant with respect to change $j_z\to -j_z$. Therefore the states with the projections of the total angular momentums $j_z=-j_z$ are Kramers doublets.

B. Electron energy levels in quantizing magnetic field

In the presence of a strong magnetic field the electronic levels split into Landau levels. In the case of DMS QD in a strong magnetic field both exchange and Landau splitting of electron states take place.

When we include a quantizing uniform magnetic field $\mathbf{H}=(0,0,H)$ along the growth direction z, described by the vector potential

$$\mathbf{A}=\left(-\frac{Hy}{2},\frac{Hx}{2},0\right), \quad (41)$$

the operators $k_\pm$ in Eqs. (3) and (14) become cylindrical coordinates and take the form

$$k_\pm=-ie^{\pm i\varphi}\left(\frac{d}{d\rho}\pm i\frac{1}{\rho}\frac{d}{d\varphi}\mp\frac{\rho}{2\alpha^2}\right), \quad (42)$$

where $\alpha=\sqrt{\frac{\hbar c}{eH}}$ is the magnetic length.

If a strong magnetic field is applied along the z direction the Zeeman term, H_z, in the Hamiltonian (12) has the following form in terms of the Bloch functions (2).

$$H_Z=s_H\begin{pmatrix}1/2&0&0&0&0&0&0&0\\0&-1/2&0&0&0&0&0&0\\0&0&1/2&0&0&0&0&0\\0&0&0&1/6&0&0&-\sqrt{2}/3&0\\0&0&0&0&-1/6&0&0&\sqrt{2}/3\\0&0&0&0&0&-1/2&0&0\\0&0&0&-\sqrt{2}/3&0&0&-1/6&0\\0&0&0&0&\sqrt{2}/3&0&0&1/6\end{pmatrix}, \quad (43)$$

where

$$s_H = g_0 \mu_B H, \tag{44}$$

g_0 is the free electron g-factor.

The eight-band Kane model used to describe the electron energy spectra in most direct gap semiconductors gives the following dependence of the electron g-factor on its energy ε:[40,41]

$$g(\varepsilon) = g_0 - \frac{2E_p}{3}\frac{\Delta}{(\varepsilon_g + \varepsilon)(\varepsilon_g + \varepsilon + \Delta)}.$$

Here E_p is the Kane energy parameter, and $g_0=2$ is the free electron g-factor. The second term describes the negative contribution of the valence band (with $\Delta>0$) into the electron g-factor [the value of $g(\varepsilon)$ is different from g_0 only in the presence of spin -orbit splitting]. In order not to take twice into account the negative contribution of the valence bands into the electron g-factor in quantizing magnetic field we had to set $g_0=2$ in our calculations.

Since the system is cylindrically symmetric the wave functions in quantizing magnetic field can be represented as

$$\begin{pmatrix} \Psi_1(\rho,\varphi) \\ \Psi_2(\rho,\varphi) \end{pmatrix} = \begin{pmatrix} e^{im\varphi} e^{-x/2} x^{|m|/2} Y(x) \\ e^{i(m+1)\varphi} e^{-x/2} x^{|m+1|/2} Z(x) \end{pmatrix}, \tag{45}$$

where

$$x = \frac{\rho^2}{2\alpha^2}. \tag{46}$$

Using Eqs. (42) and (45) one can obtain the following system of second-order ordinary differential equations:

$$\begin{aligned} & x\frac{d^2Y(x)}{dx^2} + (1 - x + |m|)\frac{dY(x)}{dx} - \frac{1}{2}(r_1 - \varepsilon_1 - h_1 + 1 + |m| + m) \\ & \times Y(x) + \frac{\sqrt{2}}{2} R_1 x^{(|m+1|-|m|+1)/2} \\ & \times \left(\frac{dZ(x)}{dx} + \frac{|m+1| + m + 1}{2x} Z(x) \right) = 0, \end{aligned}$$

$$\begin{aligned} & x\frac{d^2Z(x)}{dx^2} + (1 - x + |m+1|)\frac{dZ(x)}{dx} \\ & - \frac{1}{2}(2 + m + |m+1| + h_2 - \varepsilon_2 - r_2) Z(x) \\ & - \frac{\sqrt{2}}{2} R_2 x^{(|m|-|m+1|+1)/2} \\ & \times \left(\frac{dY(x)}{dx} + \frac{|m| - m - 2x}{2x} Y(x) \right) = 0. \end{aligned} \tag{47}$$

In Eqs. (47) we have introduced dimensionless parameters:

$$r_1 = \frac{(3Ar + s_H/2)\alpha^2}{P^2\left(\frac{1}{2L_H^+} + \frac{F_H^- + 2L_H^-}{6(D_H^+ M_H^- - 2T_H^2)} \right)}, \tag{48}$$

$$r_2 = \frac{(3Ar + s_H/2)\alpha^2}{P^2\left(\frac{1}{2L_H^+} + \frac{F_H^- + 2L_H^-}{6(D_H^+ M_H^- - 2T_H^2)} \right)}, \tag{49}$$

$$\varepsilon_1 = \frac{\varepsilon\alpha^2}{P^2\left(\frac{1}{2L_H^-} + \frac{F_H^+ + 2L_H^+}{6(D_H^- M_H^+ - 2T_H^2)} \right)} - \frac{\frac{(2F_H^+ + L_H^+)\langle k_z^2 \rangle \alpha^2}{3(D_H^+ M_H^- - 2T_H^+)}}{\left(\frac{1}{2L_H^-} + \frac{F_H^+ + 2L_H^+}{6(D_H^- M_H^+ - 2T_H^2)} \right)}, \tag{50}$$

$$\varepsilon_2 = \frac{\varepsilon\alpha^2}{P^2\left(\frac{1}{2L_H^+} + \frac{F_H^- + 2L_H^-}{6(D_H^+ M_H^- - 2T_H^2)} \right)} - \frac{\frac{(2F_H^- + L_H^-)\langle k_z^2 \rangle \alpha^2}{3(D_H^- M_H^+ - 2T_H^2)}}{\left(\frac{1}{2L_H^+} + \frac{F_H^- + 2L_H^-}{6(D_H^+ M_H^- - 2T_H^2)} \right)}, \tag{51}$$

$$R_1 = \frac{\gamma\alpha}{P\left(\frac{1}{2L_H^-} + \frac{F_H^+ + 2L_H^+}{6(D_H^- M_H^+ - 2T_H^2)} \right)}, \tag{52}$$

$$R_2 = \frac{\gamma\alpha}{P\left(\frac{1}{2L_H^+} + \frac{F_H^- + 2L_H^-}{6(D_H^+ M_H^- - 2T_H^2)} \right)}, \tag{53}$$

and

$$h_1 = \frac{6T_H^2 + L_H^-(F_H^+ + 2L_H^+) - 3D_H^- M_H^+}{6T_H^2 - L_H^-(F_H^+ + 2L_H^+) - 3D_H^- M_H^+}, \tag{54}$$

$$h_2 = \frac{6T_H^2 + L_H^+(F_H^- + 2L_H^-) - 3D_H^+ M_H^-}{6T_H^2 - L_H^+(F_H^- + 2L_H^-) - 3D_H^+ M_H^-}, \tag{55}$$

where

$$D_H^\pm = D^\pm \pm \frac{s_H}{6}, \tag{56}$$

$$F_H^\pm = F^\pm \pm \frac{s_H}{2}, \tag{57}$$

$$L_H^\pm = L^\pm \pm \frac{s_H}{2}, \tag{58}$$

$$M_H^\pm = M^\pm \pm \frac{s_H}{6}, \tag{59}$$

$$T_H = T + \frac{s_H}{3}. \tag{60}$$

Let a_1 and a_2 be determined by the following equations:

$$x\frac{d^2Y(x)}{dx^2}+(1+|m|-x)\frac{dY(x)}{dx}-a_1Y(x)=0, \tag{61}$$

$$x\frac{d^2Z(x)}{dx^2}+(1+|m+1|-x)\frac{dZ(x)}{dx}-a_2Y(x)=0. \tag{62}$$

Upon substitution of Eqs. (61) and (62) into Eqs. (47) we get

$$\begin{aligned}&a_1Y(x)-\frac{1}{2}(r_1-\varepsilon_1-h_1+1+|m|+m)Y(x)\\&+R_1\frac{\sqrt{2}}{2}\left(\frac{dZ(x)}{dx}+\frac{|m+1|+m+1}{2x}Z(x)\right)\\&\times x^{(|m+1|-|m|+1)/2}=0,\end{aligned}$$

$$\begin{aligned}&a_2Z(x)-\frac{1}{2}(2+m+|m+1|+h_2-\varepsilon_2-r_2)Z(x)\\&-R_2\frac{\sqrt{2}}{2}\left(\frac{dY(x)}{dx}+\frac{|m|-m-2x}{2x}Y(x)\right)x^{(|m|-|m+1|+1)/2}=0.\end{aligned} \tag{63}$$

The bounded solutions of Eqs. (63) are

$$\begin{pmatrix}Y(x)\\Z(x)\end{pmatrix}=\begin{pmatrix}d_1M(a_1,b_1,x)\\d_2M(a_2,b_2,x)\end{pmatrix}, \tag{64}$$

where $M(a,b,x)$ is a confluent hypergeometric function. Using standard properties of confluent hypergeometric functions[34] we have

$$a_1^{\pm}=\begin{cases}m-\eta^{\pm}, & \text{for } m\geqslant 0\\ -\eta^{\pm}, & \text{for } m<0,\end{cases} \tag{65}$$

$$a_2^{\pm}=\begin{cases}m-\eta^{\pm}, & \text{for } m\geqslant 0\\ -\eta^{\pm}-1, & \text{for } m<0,\end{cases} \tag{66}$$

$$b_1=\begin{cases}m+1, & \text{for } m\geqslant 0\\ |m|+1, & \text{for } m<0,\end{cases} \tag{67}$$

$$b_2=\begin{cases}m+2, & \text{for } m\geqslant 0\\ |m|, & \text{for } m<0,\end{cases} \tag{68}$$

where the dimensionless energy parameter $\eta^{\pm}$ is defined as

$$\begin{aligned}\eta^{\pm}=\frac{1}{8}\{&-8-2r_1+2r_2+2R_1R_2+2\varepsilon_1+2\varepsilon_2+2h_1-2h_2\\&\pm[(-8-2r_1+2r_2+2R_1R_2+2\varepsilon_1+2\varepsilon_2+2h_1-2h_2)^2\\&+16(-3-3r_1+r_2+r_1r_2+2R_1R_2+3\varepsilon_1-r_2\varepsilon_1+\varepsilon_2\\&+r_1\varepsilon_2-\varepsilon_1\varepsilon_2+3h_1-r_2h_1-\varepsilon_2h_1-h_2-r_1h_2\\&+\varepsilon_1h_2+h_1h_2)]^{1/2}\}.\end{aligned} \tag{69}$$

As a result, for each given energy value ε there exist two independent solutions for η. Expressing the radial wave function as a linear combination of these two independent solutions allows us to satisfy the boundary conditions. These solutions can be written as

$$\begin{aligned}f(x)=&\tilde{A}d_1^+e^{-x/2}x^{m/2}M(m-\eta^+,m+1,x)\\&+\tilde{B}d_1^-e^{-x/2}x^{m/2}M(m-\eta^-,m+1,x),\\g(x)=&\tilde{A}d_2^+e^{-x/2}x^{(m+1)/2}M(m-\eta^+,m+2,x)\\&+\tilde{B}d_2^-e^{-x/2}x^{(m+1)/2}M(m-\eta^-,m+2,x)\quad \text{for } m\geqslant 0\end{aligned} \tag{70}$$

and

$$\begin{aligned}f(x)=&\tilde{A}d_1^+e^{-x/2}x^{|m|/2}M(-\eta^+,1+|m|,x)\\&+\tilde{B}d_1^-e^{-x/2}x^{|m|/2}M(-\eta^-,1+|m|,x),\\g(x)=&\tilde{A}d_2^+e^{-x/2}x^{(|m|-1)/2}M(-\eta^+-1,|m|,x)\\&+\tilde{B}d_2^-e^{-x/2}x^{(|m|-1)/2}M(-\eta^--1,|m|,x)\quad \text{for } m<0.\end{aligned} \tag{71}$$

In a quantum dot the boundary condition $f(x=x_0)=g(x=x_0)=0$ (where $x_0=\frac{r_0^2}{2\alpha^2}$) gives us the following equations for energy spectrum of a DMS quantum dot:

$$\begin{aligned}&\frac{\left(-\frac{1}{2}-\eta^--\frac{1}{2}(r_1-\varepsilon_1-h_1)\right)}{\left(-\frac{1}{2}-\eta^+-\frac{1}{2}(r_1-\varepsilon_1-h_1)\right)}M\left(m-\eta^+,m+1,\frac{r_0^2}{2\alpha^2}\right)\\&\times M\left(m-\eta^-,m+2,\frac{r_0^2}{2\alpha^2}\right)-M\left(m-\eta^-,m+1,\frac{r_0^2}{2\alpha^2}\right)\\&\times M\left(m-\eta^+,m+2,\frac{r_0^2}{2\alpha^2}\right)=0\quad \text{for } m\geqslant 0,\end{aligned} \tag{72}$$

$$\begin{aligned}&\frac{\left(-\eta^+-1-\frac{1}{2}(1+h_2-\varepsilon_2-r_2)\right)}{\left(-\eta^--1-\frac{1}{2}(1+h_2-\varepsilon_2-r_2)\right)}M\left(-\eta^+,1+|m|,\frac{r_0^2}{2\alpha^2}\right)\\&\times M\left(-\eta^--1,|m|,\frac{r_0^2}{2\alpha^2}\right)-M\left(-\eta^-,1+|m|,\frac{r_0^2}{2\alpha^2}\right)\\&\times M\left(-\eta^+-1,|m|,\frac{r_0^2}{2\alpha^2}\right)=0\quad \text{for } m<0.\end{aligned} \tag{73}$$

These equations fully describe the energy spectrum of the problem.

III. RESULTS AND DISCUSSIONS

In this section we present our numerical results on the splitting energies of the electrons in a $Cd_{1-y}Mn_yTe$ DMS quantum dot. We use the following set of bulk parameters: $m_e=0.096m_0$, where m_0 is the free electron mass. The spin-orbit splitting is $\Delta=0.953$ eV, the Kane matrix element for

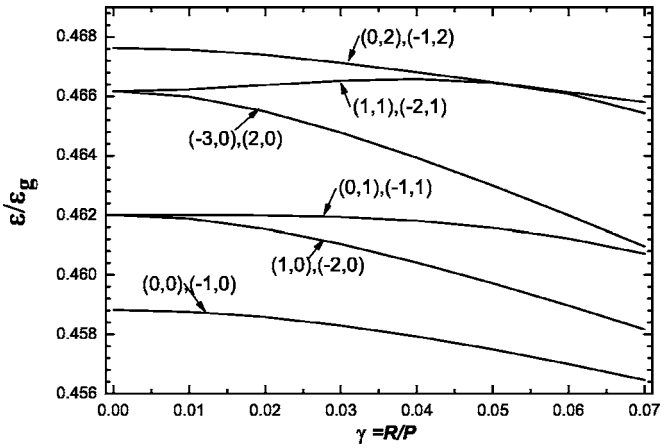

FIG. 1. Dependence of the energy levels (in ε_g units) on the dimensionless parameter γ in the absence of the Zeeman and exchange interaction term calculated using Eq. (40). The QD radius is $r_0=200$ Å and the thickness of the QD is $d=20$ Å. The Mn concentration is $y=0.02$.

the interaction between S and p bands $E_p=2m_0P^2/\hbar^2$, where $E_p=18.8$ eV. In $Cd_{1-y}Mn_yTe$ DMS the semiconductor band gap depends on the Mn concentration y: $\varepsilon_g=(\varepsilon_{g0}+1.51y)$ eV, where $\varepsilon_{g0}=1.586$ eV is the gap in the absence of Mn magnetic ions. Other parameters used in our calculations, $N_0\alpha=0.22$ eV, $N_0\beta=-0.88$ eV, are taken from the literature.[15,16]

We have analyzed Eqs. (38)–(40), (72), and (73) numerically, labeling the energy eigenstates as $\varepsilon(m,n)$, where n is a non-negative integer $(n=0,1,2,\ldots)$ and denotes the nth zeroes of these equations with fixed m. Here, we must notice that Eq. (38) is valid only when the QD radius r_0 is small compared to the magnetic length α, $r_0 \ll \alpha$.

In Fig. 1 we plot the lower energy levels as a function of dimensionless parameter $\gamma=R/P$ in the absence of the Zeeman and the exchange interaction terms using Eq. (40). The QD radius is $r_0=200$ Å and the thickness of the QD is $d=20$ Å. For $\gamma=0$ the states with the angular momentum $l=0$ (fundamental states) are twofold degenerate, but the states with $l\neq 0$ are fourfold degenerate. For $\gamma\neq 0$ the electron states with $j=l+1/2$ and $j=l-1/2$ have different energies for $l\geqslant 1$. Hence all states with $l\geqslant 1$ split into two, while $l=0$ states remain double-degenerate. In Fig. 1 the electron states (0, 0) and $(-1,0)$ correspond to the total angular momentum projection $j_z=1/2$ and $j_z=-1/2$, respectively; (1, 0) and $(-2,0)$ correspond to $j_z=3/2$ and $j_z=-3/2$, respectively; (0, 1) and $(-1,1)$ states again correspond to $j_z=1/2$ and $j_z=-1/2$, respectively; (2, 0) and $(-3,0)$ correspond to $j_z=5/2$ and $j_z=-5/2$, respectively; (1, 1) and $(-2,1)$ correspond again to $j_z=3/2$ and $j_z=-3/2$, respectively; (0, 2) and $(-1,2)$ states (second double degenerate state at $\gamma=0$) again correspond to $j_z=1/2$ and $j_z=-1/2$, respectively. In the absence of the exchange interaction term there is an additional symmetry, $j_z=-j_z$, related to the time inversion. So, in the absence of the Zeeman exchange interaction term the Rashba term partially lifts the degeneracy of levels.

In Fig. 2 we plot the electron levels as a function of the dimensionless parameter γ for the magnetic field $H=1$ T and the temperature $T=3$ K at a fixed Mn concentration $y=0.02$.

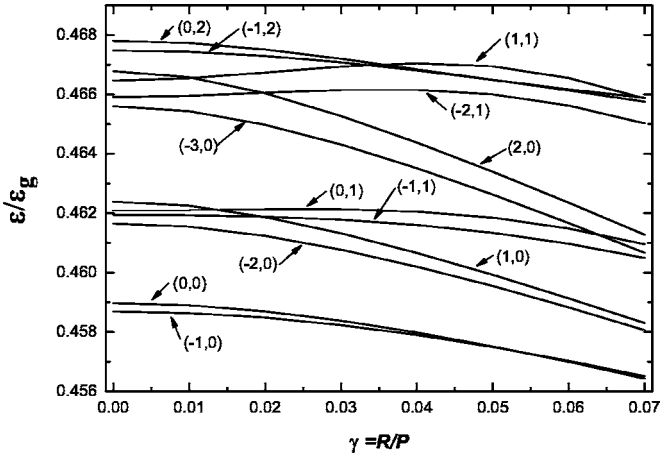

FIG. 2. Energy of low-lying states as a function of γ for $A\neq 0$ at $H=1$ T and $T=3$ K [calculated by using Eqs. (72) and (73)]. Other parameters are the same as in Fig. 1.

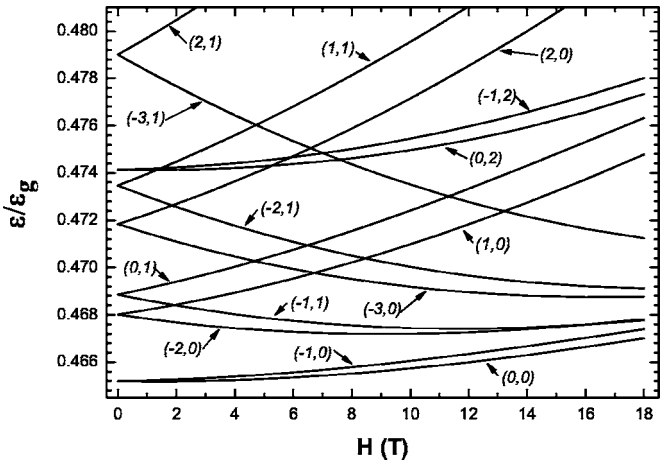

FIG. 3. Dependence of the energy levels on the strength of the magnetic field H at fixed Rashba parameter $R=2.5\times10^{-9}$ eV cm for Mn free case $y=0$. ($r_0=200$ Å, $d=20$ Å, and $T=3$ K.)

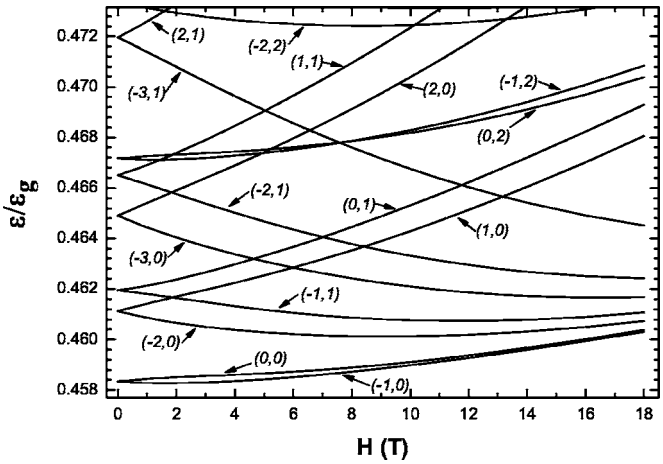

FIG. 4. The same as Fig. 3 but now for $y=0.02$.

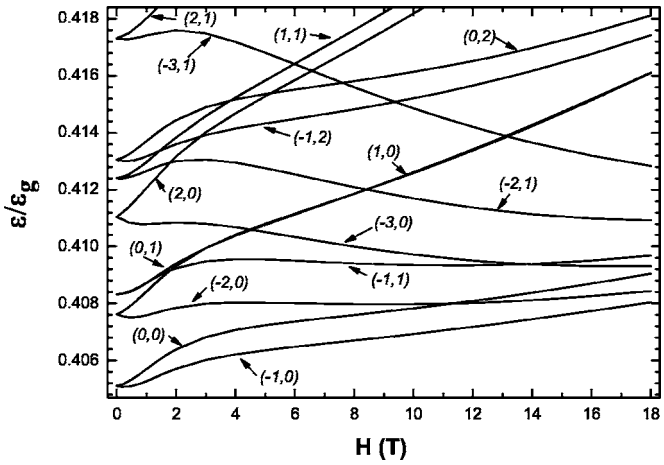

FIG. 5. The same as Fig. 3 but now for $y=0.2$.

Other parameters are the same as those of Fig. 1. With the Zeeman and the exchange interaction terms included, all Kramers doublets are also split, so that the degeneracy is completely removed. Namely, the states with quantum numbers $\pm j_z$ can have different energies.

In Figs. 3–5 we show the electron spectra of low-lying electron states in the DMS QD as a function of the magnetic field for different Mn concentrations. Experimentally observed values of Rashba spin-orbit coupling parameter R lie in the range 1–63 meV nm for a large variety of systems [for example, $In_xGa_{1-x}As/In_yAl_{1-y}As$ (Refs. 35 and 36), InAs/AlSb (Ref. 37), InAs/GaSb (Ref. 38), GaAs (Ref. 39), and InSb (Ref. 11). We assume that for a DMS QD the Rashba parameter R takes the same range of values. Here we take $R=2.5\times10^{-9}$ eV cm. The QD radius is $r_0=200$ Å and the thickness of the QD is $d=20$ Å. The results are shown for $T=3$ K. One can see in the figures one finds that the variation of the energy with the magnetic field is different from that in a DMS QD with high Mn concentration. For a nonmagnetic semiconductor (NMS) (Mn-free case, $y=0$) QD (Fig. 3) the energy levels are nearly linear at low magnetic fields. We find that in a such a case, because the Rashba

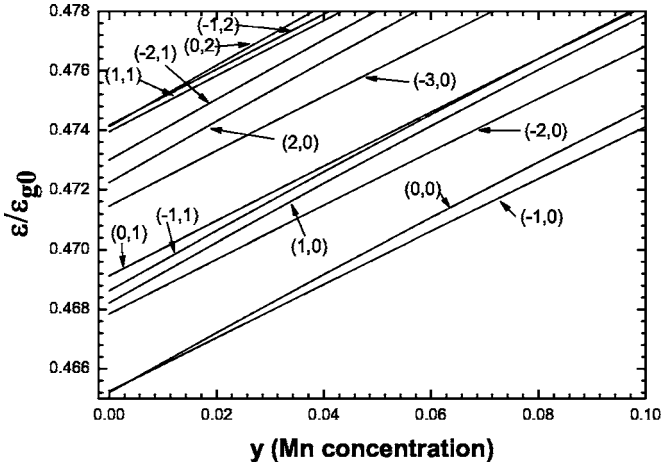

FIG. 6. Energy of low-lying levels (in $\varepsilon_{g0}=1.586$ eV units) as a function of Mn concentration at $H=1$ T, with fixed $R=2.5\times10^{-9}$ eV cm, $r_0=200$ Å, $d=20$ Å, and $T=3$ K.

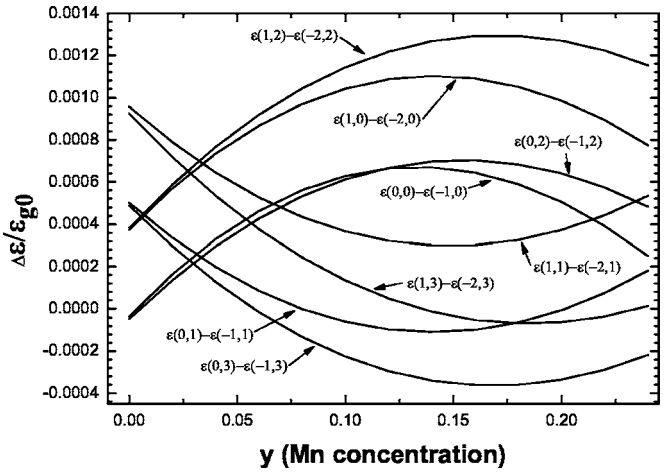

FIG. 7. The energy difference of splitting levels as a function of Mn concentration. Other parameters are the same as in Fig. 6.

parameter, R, is relatively small, the electronic levels in the high magnetic field regime are mainly determined by the Zeeman term. For the DMS QD with high Mn concentration the dependence of energy levels on the magnetic field strength is much more complicated (Fig. 5). At small magnetic fields the energy levels are determined by the exchange interaction term, the Rashba term, and the Zeeman term, for spin-up and spin-down states. The energy levels exhibit the behavior of the Brillion function since the $sp-d$ exchange interaction is the dominant factor at low magnetic fields. At large magnetic field the exchange term saturates and the energy levels are determined mainly by the Zeeman term. At high magnetic fields the energies approach the Landau levels.

In Fig. 6 we plot the low-lying energy levels (in $\varepsilon_{g0}=1.586$ eV units) as a function of Mn concentration. The value of the magnetic field is fixed at $H=1$ T. From this figure we notice that the energy of the levels increases with increasing Mn concentration. This characteristic behavior arises from the fact that the $sp-d$ exchange interaction energy is directly proportional to Mn concentration. Figure 7

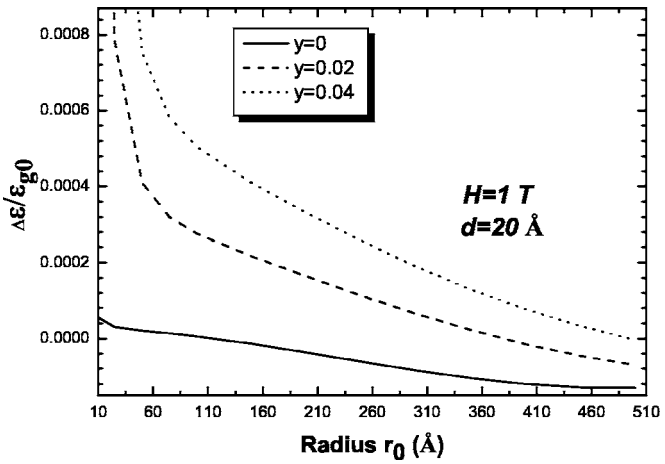

FIG. 8. The energy difference of splitting levels $\varepsilon(0,0)-\varepsilon(-1,0)$ as a function of QD radius for different Mn concentrations at $H=1$ T. ($d=20$ Å, $T=3$ K, and $R=2.5\times10^{-9}$ eV cm.)

shows the spin splitting (energy difference) as a function of Mn concentration. We see that the spin splitting increases (decreases) with increasing Mn concentration and goes through a maximum (a minimum) at high Mn concentration.

In Fig. 8 we plot the energy difference $\varepsilon(0,0)-\varepsilon(-1,0)$ (in ε_{g0} units) as a function of QD radius for different Mn concentrations. The splitting energy decreases as the QD radius increases and increases with increasing Mn concentration at fixed magnetic field.

IV. CONCLUSIONS

We calculated the electronic structure of a $Cd_{1-y}Mn_yTe$ DMS QD with Rashba spin-orbit coupling in non- and quantizing magnetic fields. The calculations are based on the eight-band $\mathbf{k}\cdot\mathbf{p}$ theory, which takes into account the nonparabolicity of the electron energy levels. The calculations also provide a description of the limiting case for zero magnetic field. A nonzero magnetic field breaks the time-inversion symmetry and removes the corresponding degeneracy. We investigated the electron levels as a function of dimensionless parameter $\gamma=R/P$ in zero and nonzero magnetic fields, as well as the magnetic field dependence of the levels for different Mn concentrations at a fixed Rashba parameter. In different magnetic field regimes and Mn concentrations the energy levels have different dependence on the magnetic field.

*Electronic address: semic@lan.ab.az; bachschi@yahoo.de

[1] S. Datta and B. Das, Appl. Phys. Lett. **56**, 665 (1990).
[2] G. Lommer, F. Malcher, and U. Rossler, Phys. Rev. Lett. **60**, 728 (1988).
[3] E. I. Rashba, Fiz. Tverd. Tela (Leningrad) **2**, 1224 (1960); Sov. Phys. Solid State **2**, 1109 (1960).
[4] W. Hausler, Phys. Rev. B **63**, 121310(R) (2001).
[5] F. Mireles and G. Kirczenow, Phys. Rev. B **64**, 024426 (2001).
[6] M. Governale and U. Zülicke, Phys. Rev. B **66**, 073311 (2002).
[7] T. Schäpers, J. Knobbe, and V. A. Guzenko, Phys. Rev. B **69**, 235323 (2004).
[8] O. Voskoboynikov, C. P. Lee, and O. Tretyak, Phys. Rev. B **63**, 165306 (2001).
[9] M. Governale, Phys. Rev. Lett. **89**, 206802 (2002).
[10] M. Valin-Rodriguez, A. Puente, and L. Serra, Phys. Rev. B **69**, 085306 (2004).
[11] C. F. Destefani, S. E. Ulloa, and G. E. Marques, Phys. Rev. B **69**, 125302 (2004).
[12] E. N. Bulgakov and A. F. Sadreev, JETP Lett. **73**, 505 (2001).
[13] E. Tsitsishvili, G. S. Lozano, and A. O. Gogolin, Phys. Rev. B **70**, 115316 (2004).
[14] F. M. Hashimzadea, A. M. Babayev, S. Cakmak, and S. Cakmaktepe, Physica E (Amsterdam) **25**, 78 (2004).
[15] K. Furdyna, J. Appl. Phys. **64**, R29 (1988).
[16] P. A. Wolff, in *Semiconductors and Semimetals, Diluted Magnetic Semiconductors*, edited by J. K. Furdyna and J. Kossut (Academic, New York, 1988).
[17] N. B. Brandt and V. V. Moshchalkov, Adv. Phys. **33**, 193 (1984).
[18] H. Xin, P. D. Wang, A. Yin, C. Kim, M. Dobrowolska, J. L. Merz, and J. K. Furdyna, Appl. Phys. Lett. **69**, 3884 (1996).
[19] Y. Oka, J. Shen, K. Takabayashi, N. Takahashi, H. Mitsu, I. Souma, and R. Pittini, J. Lumin. **83**, 83 (1999).
[20] C. S. Kim, M. Kim, S. Lee, J. Kossut, J. K. Furdyna, and M. Dobrowolska, J. Cryst. Growth **214**, 395 (2000).
[21] A. A. Maksimov, G. Bacher, A. McDonald, V. D. Kulakovskii, A. Forchel, C. R. Becker, G. Landwehr, and L. Molenkamp, Phys. Rev. B **62**, R7767 (2000).
[22] G. Bacher, H. Schomig, M. K. Welsch, S. Zaitsev, V. D. Kulakovskii, A. Forchel, S. Lee, M. Dobrowolska, J. K. Furdyna, B. Konig, and W. Ossau, Appl. Phys. Lett. **79**, 524 (2001).
[23] J. Kossut, I. Yamakawa, A. Nakamura, I. Yamakawa, A. Nakamura, and S. Takeyama, Appl. Phys. Lett. **79**, 1789 (2001).
[24] Kai Chang, J. B. Xia, and F. M. Peeters, Appl. Phys. Lett. **82**, 2661 (2003).
[25] Kai Chang, S. S. Li, J. B. Xia, and F. M. Peeters, Phys. Rev. B **69**, 235203 (2004).
[26] F. V. Kyrychenko and J. Kossut, Phys. Rev. B **70**, 205317 (2004).
[27] Kai Chang and J. B. Xia, J. Phys.: Condens. Matter **14**, 13661 (2002).
[28] E. G. Novik, A. Pfeuffer-Jeschke, T. Jungwirth, V. Latussek, C. R. Becker, G. Landwehr, H. Buhmann, and L. W. Molenkamp, Phys. Rev. B **72**, 035321 (2005).
[29] Y. A. Bychkov and E. I. Rashba, J. Phys. C **17**, 6039 (1984).
[30] R. Winkler, Phys. Rev. B **62**, 4245 (2000).
[31] G. L. Bir and G. E. Pikus, *Symmetry and Strain-Induced Effects in Semiconductors* (Nauka, Moscow, 1972).
[32] E. O. Kane, J. Phys. Chem. Solids **1**, 249 (1957).
[33] A. I. Anselm, *Introduction to Semiconductor Theory* (Nauka, Moscow, 1978).
[34] M. Abramowitz and I. A. Stegun, *Handbook of Mathematical Functions, Applied Math. Series 55* (National Bureau of Standards, 1964).
[35] B. Das, S. Datta, and R. Reifenberger, Phys. Rev. B **41**, 8278 (1990).
[36] J. Nitta, T. Akazaki, H. Takayanagi, and T. Enoki, Phys. Rev. Lett. **78**, 1335 (1997).
[37] J. P. Heida, B. J. van Wees, J. J. Kuipers, T. M. Klapwijk, and G. Borghs, Phys. Rev. B **57**, 11911 (1998).
[38] J. Luo, H. Munekata, F. F. Fang, and P. J. Stiles, Phys. Rev. B **41**, 7685 (1990).
[39] A. V. Khaetskii and Yu. V. Nazarov, Phys. Rev. B **61**, 12639 (2000).
[40] L. M. Roth, B. Lax, and S. Zwerdling, Phys. Rev. **114**, 90 (1959).
[41] C. Hermann and C. Weisbuch, Phys. Rev. B **15**, 823 (1977).
[42] M. I. Dyakonov and T. M. Kocharovski, Fiz. Tekh. Poluprovodn. (S.-Peterburg) **20**, 178 (1986) [Sov. Phys. Semicond. **20**, N1 (1986)].